Microscopic evidence for the stacking faults and metallic properties of a triangular lattice CoO_2 with a three-layer structure

2010 J. Phys.: Condens. Matter 22 035602

(http://iopscience.iop.org/0953-8984/22/3/035602)

J. Phys.: Condens. Matter **22** (2010) 035602 (6pp) doi:10.1088/0953-8984/22/3/035602

Microscopic evidence for the stacking faults and metallic properties of a triangular lattice CoO_2 with a three-layer structure

Masashige Onoda and Asami Sugawara

Institute of Physics, University of Tsukuba, Tennodai, Tsukuba 305-8571, Japan

E-mail: onoda.masashige.ft@u.tsukuba.ac.jp

Received 24 July 2009, in final form 27 November 2009
Published 21 December 2009
Online at stacks.iop.org/JPhysCM/22/035602

Abstract

Stacking faults and metallic properties for the triangular lattice system CoO_2, which has basically three oxygen layers with a prismatic oxygen environment between the layers, have been explored mainly through measurements of nuclear magnetic and quadrupole resonance. A significant distribution of the quadrupole frequency for ^{59}Co nuclei, due to stacking faults and short atomic coherence, is found. The spin dynamics is successfully understood in terms of the relaxation mechanism for a weakly correlated metal system.

1. Introduction

Transition-metal oxides and the nonstoichiometric bronzes have been investigated for a long time from both the basic science and applied viewpoints. For example, the proposal of a resonating-valence-bond theory for a triangular lattice system with Heisenberg interaction [1, 2] aroused considerable interest in geometrically frustrated spin systems. The discovery of superconductivity in $Na_xCoO_2{\cdot}yH_2O$ with a transition temperature $T_c \approx 5$ K, where $x \simeq 0.3$ and $y \simeq 1.3$ [3], as well as the possible application to thermoelectric devices in the parent compound Na_xCoO_2 [4] has accelerated investigations of the triangular lattice system.

Na_xCoO_2 has a crystal structure, basically described in terms of CoO_6 octahedra which are joined by sharing edges to form a two-dimensional triangular lattice of Co ions [5]. Much work on the triangular lattice Co oxides is performed for the γ phase, which has a two-layer structure with a trigonal prismatic environment for Na, and is defined as the 'P2' structure. On increasing x from $\approx$0.3 to $\approx$0.8 in the P2 phase, the ground state goes from a normal metal to a Curie–Weiss metal via a poor metallic state at $x \approx 0.5$, accompanied with a partial valence order of Co [5, 6]. Recently, a new type of the triangular lattice $H_{0.3}CoO_2$, prepared by soft-chemistry synthesis, was found to have a P2 structure and to exhibit weakly correlated or normal metallic properties [7].

The Li_xCoO_2 system is a well-known triangular lattice oxide from being one of the excellent Li rechargeable batteries [8]. The structure for $x = 1$ is an α-$NaFeO_2$ type with an octahedral coordination for alkali atoms and three layers of oxygens, which is called 'O3'. The structural aspects and the metal–insulator transitions in the Li de-intercalated process have been studied, especially relating to the performance of batteries.

CoO_2 is the parent compound for Na_xCoO_2 and Li_xCoO_2. Here, two kinds of phases exist. The compound prepared with an electrochemical de-intercalation of Li for $LiCoO_2$ has a CdI_2-type 'O1' structure with space group $P\bar{3}m1$ and cell dimensions of $a = 2.822$ and $c = 4.293$ Å [9]. On the other hand, a soft-chemical synthesis with H_2SO_4 provides a 'P3'-type stacking fault structure with shift vectors $\boldsymbol{s}_1 = \frac{2}{3}\boldsymbol{a} + \frac{1}{3}\boldsymbol{b}$ and $\boldsymbol{s}_2 = \frac{1}{3}\boldsymbol{a} + \frac{2}{3}\boldsymbol{b}$ along the shift of $\frac{1}{3}\boldsymbol{c}$, where the basic space group is centrosymmetric $R\bar{3}m$ and the cell dimensions are $a = 2.839$ and $c = 13.439$ Å [10]. Hereafter, the CoO_2 compounds with O1 and P3 structures are referred to as CoO_2 (O1) and CoO_2 (P3), respectively, where the Co ions may be in a low-spin $3d^5$ configuration due to the strong crystal field. A nuclear magnetic resonance (NMR) study for CoO_2 (O1) reveals a metallic ground state [11, 12]. CoO_2 (P3) is also found to exhibit metallic properties on the basis of results for the thermoelectric power and the magnetic susceptibility [10]. Superconductivity emerges around $Na_{0.3}CoO_2$ when water molecules are intercalated in between the Co layers.

In order to clarify further the structural and electronic properties of CoO_2 (P3), NMR and nuclear quadrupole

resonance (NQR) are primarily performed together with measurements of x-ray diffraction, electrical resistivity, thermoelectric power and magnetic susceptibility. The details regarding the sample preparation and the measurements are given in section 2. The results and discussions are presented in section 3. Section 4 is devoted to conclusions.

2. Experiments

Polycrystalline specimens of CoO_2 (P3) were synthesized by the soft-chemistry method described previously [10]: $\sim 1.5 \times 10^{-3}$ kg of $LiCoO_2$ was mixed with 300 ml of 10 mol l^{-1} of H_2SO_4 through 6 days of stirring, where H_2SO_4 was repurified every other day, and then by washing the product with water and drying in air, powder specimens were obtained. For measurements of the physical properties, the specimens were pressed into pellets at a pressure of 2.5×10^7 N m^{-2}.

For the two kinds of polycrystalline specimens of CoO_2 (P3), hereafter referred to as CoO_2 (P3)#1 and #2, the following measurements were performed. Inductively coupled plasma-optical emission spectroscopy (ICP) was done using a Nippon Jarrell-Ash ICAP-575 spectrometer. An x-ray powder diffraction pattern was taken with Cu Kα radiation at 293 K using a Rigaku RAD-IIC diffractometer. The four-terminal electrical resistivity and the thermoelectric power were measured with the dc method at temperatures between 4.2 and 300 K. The magnetization measurements were done at temperatures between 4.2 and 300 K by the Faraday method with a field of up to 1 T. The magnetic susceptibility was deduced from the linear part of the magnetization–field curve with a decreasing field. The NMR and NQR measurements of the ^{59}Co nuclei were performed with a standard coherent pulsed technique in the temperature region between 4.5 and 40 K. The spectra were taken by recording the spin-echo intensities with the magnetic field or frequency varied stepwise. The NMR measurements of the ^{7}Li nuclei in a small amount of the second phase of the specimens were also done by the Fourier transform (FT) technique. The spin–lattice relaxation time was measured by monitoring the recovery of the spin-echo intensities with the standard inversion-recovery pulse sequence.

3. Results and discussions

3.1. Chemical analyses and structural aspects

On the basis of ICP analysis, 0.040 and 0.026 Li ions per Co are detected for CoO_2 (P3)#1 and #2, respectively. Although the x-ray diffraction patterns for #1 and #2 are almost understood from those having light stacking faults for the c-direction as pointed out previously [10], they contain a very small amount of a second phase of the O3-type triangular lattice compound Li_xCoO_2 and the spinel-type Co_3O_4, respectively. Since the preparation methods for CoO_2 (P3)#1 and #2 are the same, the appearance of different second phases is accidental. The phases of Li_xCoO_2 (O3) and Co_3O_4 likely come from the incomplete soft-chemical and solid-state reactions of $LiCoO_2$, respectively.

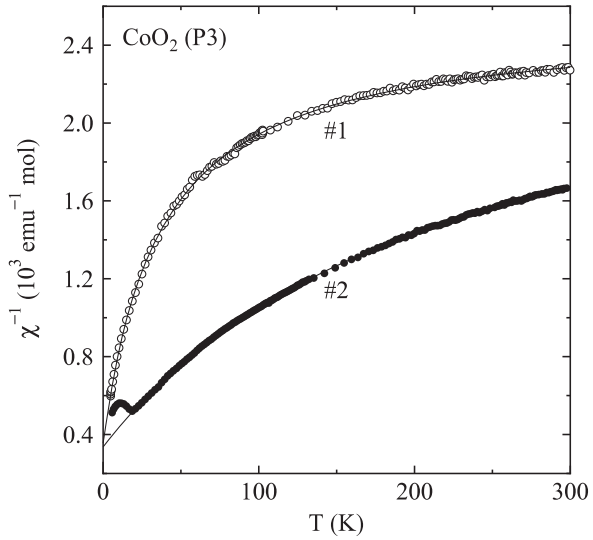

Figure 1. The temperature dependences of the inverse magnetic susceptibilities for CoO_2 (P3)#1 and #2, where the full curves denote fits to equation (1) with the parameters in table 1.

3.2. Transport and magnetic properties

The electrical resistivities and the thermoelectric powers for CoO_2 (P3)#1 and #2 are confirmed to agree with the previous data [10]: that is, the resistivities that apparently show a nonmetallic behaviour are explained with a parallel combination of the Fermi-liquid transport and the variable-range hopping transport in three dimensions due to the loose packing of specimens. The thermoelectric powers that have magnitudes smaller than 10 μV K^{-1} and a dependence linear in temperature above 50 K, below which they are nearly zero, are also understood basically with the Fermi-liquid model for hole carriers.

The magnetic susceptibilities χ as a function of temperature for CoO_2 (P3)#1 and #2 are shown in figure 1. As the temperature is lowered, the susceptibility of CoO_2 (P3)#1 increases without any anomaly, which is similar to the previous results [10]. The data for #2 increases at temperatures above 15 K and then exhibits a maximum, likely corresponding to the antiferromagnetic order. The paramagnetic behaviours are well fitted with the Curie–Weiss law,

$$\chi = C/(T + T_W) + \chi_0, \quad (1)$$

where C, T_W and χ_0 are the Curie constant, the Weiss temperature and the temperature-independent susceptibility, respectively. The full curves shown in figure 1 provide parameters listed in table 1. Since the Curie constant for CoO_2 (P3)#1 is about 3% of the value for $S = \frac{1}{2}$ and $g = 2$, the temperature-dependent contribution may be attributed to impurities and/or lattice imperfections. On the other hand, C for CoO_2 (P3)#2 is about 20% of the free-spin value and T_W is not so small. Since CoO_2 (P3)#2 has a minor phase of Co_3O_4, as described before, the temperature-dependent susceptibility and its maximum phenomenon of CoO_2 (P3)#2 likely come from Co_3O_4. It is known that

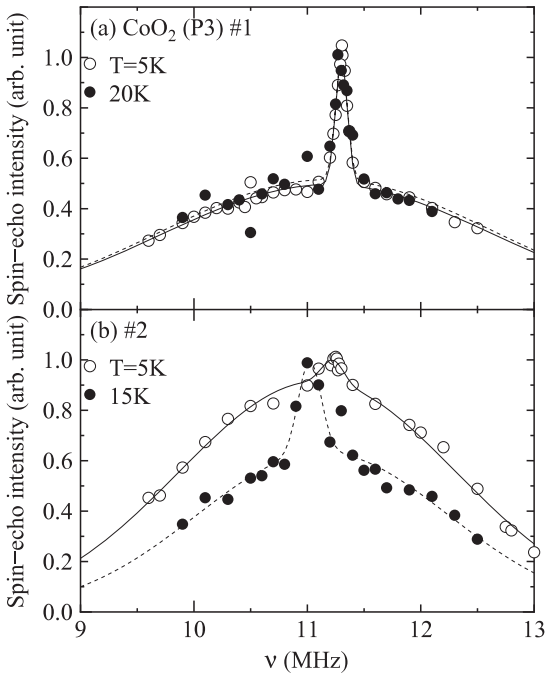

Figure 2. (a) The NQR spectra of ^{59}Co nuclei for the transition of $\Delta m = \pm\frac{5}{2} \leftrightarrow \pm\frac{7}{2}$ at 5 and 20 K for CoO_2 (P3)#1; and (b) those at 5 and 15 K for #2. Here, the full and dotted curves indicate fits to a Gaussian, whose parameters at 5 K are listed in table 2.

Table 1. The parameters of magnetic susceptibilities for CoO_2 (P3)#1 and #2.

	C (emu K mol^{-1})	T_W (K)	χ_0 (10^{-4} emu mol^{-1})
CoO_2 (P3)#1	0.0124(1)	5.1(1)	3.96(1)
CoO_2 (P3)#2	0.0744(3)	28.6(3)	3.73(1)

Co_3O_4 exhibits antiferromagnetism with the Néel temperature at $T_N \simeq 30$ K [13, 14]. Here, the Co^{3+} ions at the octahedral B sites are diamagnetic, and the Co^{2+} ions with $S = \frac{3}{2}$ and $g = 2.17$ at the tetrahedral A sites form an antiferromagnetic sublattice with the diamond structure below T_N. The reason why Co_3O_4 contained in CoO_2 (P3)#2 has T_N of about 15 K lower than the original value is likely that the compound is a little intercalated with Li, which is consistent with the NMR results for ^{7}Li described in section 3.4.

The constant susceptibility χ_0 in equation (1) is written as

$$\chi_0 = \chi_s + \chi_{orb} + \chi_{dia}, \tag{2}$$

where the subscripts of s, orb and dia denote the contributions from Pauli-type spin paramagnetism, orbital paramagnetism and diamagnetism, respectively. A tentative assumption that the magnitude of $\chi_{orb} + \chi_{dia}$ is the order of 10^{-5} emu mol^{-1} with $\chi_{dia} = -4.9 \times 10^{-5}$ emu mol^{-1} and the density of states $N(E_F)$ is 4.5 eV^{-1} [15] provides an effective electron mass ratio of about 3 for both of the specimens [10]. In section 3.3, the magnitudes of χ_s and χ_{orb} will be reconsidered based on the NMR and NQR results for ^{59}Co.

Table 2. The Gaussian parameters of ^{59}Co-NQR spectra and the quadrupole frequencies of the A-line for CoO_2 (P3)#1 and #2 at 5 K.

	A-line			B-line	
	ν_c (MHz)	ν_Q (MHz)	$w_{1/2}$ (MHz)	ν_c (MHz)	$w_{1/2}$ (MHz)
CoO_2 (P3)#1	11.18(3)	3.822(9)	2.91(9)	11.301(2)	0.104(3)
CoO_2 (P3)#2	11.09(2)	3.791(5)	2.45(5)	11.22(3)	0.19(6)

3.3. NMR and NQR of ^{59}Co

The NQR spectra of the ^{59}Co nuclei for CoO_2 (P3)#1 and #2 are shown in figures 2(a) and (b), respectively. Both spectra have two Gaussian components with large and small linewidths, hereafter referred to as A- and B-lines, respectively. The ratio of the intensity of B-line to that of A-line is smaller than 3%. For both lines for #1 and the A-line for #2, the centre frequency ν_c and the full width at the half maximum $w_{1/2}$ are temperature independent. Only the B-line for #2 changes with temperature. The Gaussian parameters of ν_c and $w_{1/2}$ at 5 K are listed in table 2. Judging from the magnitude of ν_c of ^{59}Co in $Na_xCoO_2{\cdot}yH_2O$ prepared with the soft-chemistry method [16], the A-line is considered to come from the transition of $\Delta m = \pm\frac{5}{2} \leftrightarrow \pm\frac{7}{2}$, which is consistent with the analysis of NMR spectra, as will be described later. The B-line is also expected to result in the same transition. Here, ν_c is defined as [17]

$$\nu_c \simeq 3\nu_Q(1 - \eta^2/10), \tag{3}$$

with the quadrupole frequency ν_Q expressed by

$$\nu_Q = 3e^2qQ/[2I(2I-1)h], \tag{4}$$

where e is the electron charge, eq is the field gradient for the Z-direction of the electric field gradient tensor, Q is the quadrupole moment, I is the nuclear spin $\frac{7}{2}$ in this case and h is the Planck constant. The large width of the A-line, where $w_{1/2}$ is about one-fourth of ν_c, may be related to the disorder introduced by the stacking fault and the short atomic coherence. On the other hand, the B-line may be a contribution from the minor phase: that is, the O3-type Li_xCoO_2 for #1 and the Li-intercalated Co_3O_4 for #2. The small width of the B-line suggests these minor phases to be free of defects, which is reasonable considering their formation process described in section 3.1.

The field swept NMR spectra of ^{59}Co nuclei for CoO_2 (P3)#1 and #2 at the Larmor frequencies $\nu_L = 47.48$ and 14.1 MHz do not depend on temperature in the temperature range measured. The spectra for #1 at 5 K and $\nu_L = 47.48$ MHz are shown in figure 3(a), and those for #1 and #2 at $\nu_L = 14.1$ MHz are in figure 3(b). The spectra for #1 agree well with those for #2, which suggests the contribution from the different minor phases to be negligibly small. Here, the small peak at $\nu_L = 14.1$ MHz and $H = 0.852$ T is attributed to the signal of ^{7}Li in the minor phase, as will be discussed in section 3.4. Thus, the NMR spectra should be explained consistently together with the NQR results for the A-line. As compared with the spectra of $Na_xCoO_2{\cdot}yH_2O$ [16],

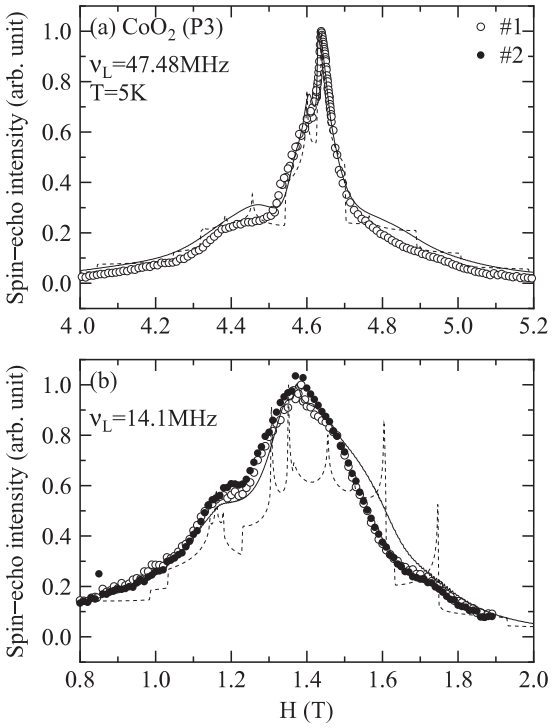

Figure 3. (a) The field swept NMR spectra of ^{59}Co nuclei for CoO_2 (P3)#1 at 5 K and $\nu_L = 47.48$ MHz, and (b) those for #1 and #2 at 5 K and $\nu_L = 14.1$ MHz. The full and dotted curves indicate results simulated in terms of a Gaussian convolution with and without taking account of the distribution of quadrupole frequency, respectively, based on the parameters given in the text.

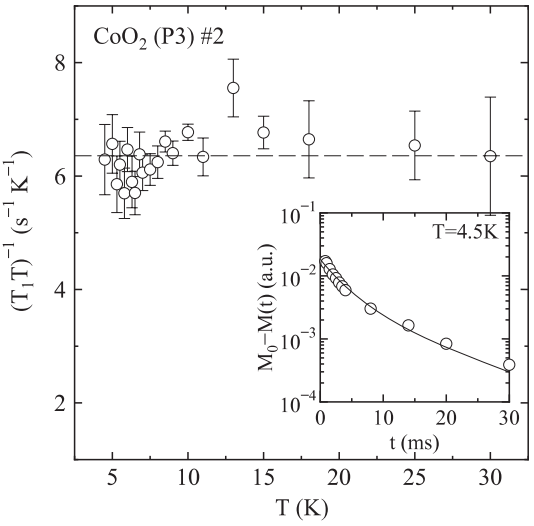

Figure 4. The temperature dependence of the inverse of the product of the spin–lattice relaxation time and the temperature of ^{59}Co nuclei for CoO_2 (P3)#2. The inset indicates the NQR decay behaviour M_0–$M(t)$ at 4.5 K with a theoretical curve, where M_0 is the saturated value.

the spectra do not have significant powder pattern singularities, which should be mainly attributed to the wide distribution of ν_Q, as pointed out from the NQR measurements.

In order to explain the NMR spectra measured at $\nu_L = 47.48$ and 14.1 MHz consistently, a pseudocontinuous normal distribution of ν_Q, based on the NQR results, is considered as follows: first, on calculating transitions which result from the spin Hamiltonian with the nuclear Zeeman, nuclear electric quadrupole and anisotropic Knight shift interactions, where the last two terms are treated as second- and first-order perturbations on the first term [18, 19], the principal axis systems of the last two tensors are assumed to be the same. Next, with the fixed asymmetry parameter of the electric field gradients η and the fixed principal values of Knight shifts K^i ($i = x$, y and z), the powder patterns for various ν_Q are calculated and they are superimposed based on a normal distribution with an adequate dispersion. Then, they are convoluted with a Gaussian with the dispersion of $(10\ \mathrm{kHz})^2$. Satisfying agreements with spectra, as shown by the full curves in figure 3, are obtained with the following parameters: the mean quadrupole frequency $\overline{\nu_Q} \simeq \nu_c/3$ with the dispersion $\sigma^2 \simeq (w_{1/2}/3)^2$ (see equation (3) and table 2), the asymmetry parameter $\eta = 0.5$, and the Knight shift parameters $K^x = 3.2$, $K^y = 2.4$ and $K^z = 2.2\%$. That is, the NMR spectra at different frequencies are fully understood with parameters determined from the NQR spectra. Using this η, ν_Q is determined as listed in table 1. For the comparison, the spectra without the distribution of ν_Q are also plotted with the dotted curves in figure 3. The present analysis of NMR spectra for materials with stacking fault and/or defect structures is considered to be useful and it sheds new light on the understanding of the electronic states.

CoO_2 may have one hole in the a_{1g} orbital for the trigonal structure. Calculating the local electric field gradient arising from the on-site hole with this wavefunction, ν_Q^{loc} is estimated to be 25.7 MHz with $\eta^{loc} = 0$ when the radical average of r^{-3} is taken to be $\langle r^{-3} \rangle = 6.699$ au [20] and the principal axis of maximum electric field gradient corresponds to the c-axis. These values are not consistent with the experimental ones, which may be partly due to the disorder effect of stacking faults. It would be also necessary to take account of the partial occupancy effect of doublet e_g orbitals. Of course, depending on the magnitude of Sternheimer antishielding factor, the electric field gradient from the ions surrounding Co should also be considered [21]. The Knight shift anisotropy suggests that the local symmetry of Co is lower than orthorhombic, which is different from the result for $Na_xCoO_2{\cdot}yH_2O$, which shows the uniaxial relation of $K^x = K^y > K^z$ [16]. In the present work, the disorder effect of stacking faults is considered to mainly contribute to the distribution of electric field gradient. However, there is additional possibility that the Knight shift anisotropy also changes more or less due to the disorder effect. So, later only the average value of the Knight shift will be discussed.

The NQR magnetizations $M(t)$ for the A-line of ^{59}Co in CoO_2 (P3)#2 are fitted to the multi-exponential relaxation curve derived theoretically [22] with a single component of the spin–lattice relaxation time T_1, as shown in the inset of figure 4. The temperature dependence of the inverse of the product of T_1 and the temperature, where the quantized axis is expected to correspond to the c-axis from the basic crystal symmetry, is shown in figure 4. In the temperature range measured, $(T_1T)^{-1}$ is nearly constant, 6.35(9) s^{-1} K^{-1}, which indicates that the

Korringa relation apparently holds, since the Knight shifts are temperature independent. This value is significantly smaller than that of CoO_2 (O1), about 20 s^{-1} K^{-1}, at temperatures below 7 K [11, 12] and is in striking contrast with that for the $Na_xCoO_2 \cdot yH_2O$ superconductor, where $(T_1T)^{-1}$ in the normal state follows a Curie–Weiss law due to antiferromagnetic spin fluctuations [16].

Let us analyse the present NMR and NQR results of ^{59}Co considering that the electron correlation for the present case is not so strong. Based on equation (2), the Knight shift is written as

$$K = K_s + K_{orb}. \tag{5}$$

Here, K_i is related to the respective susceptibility through an equation

$$K_i = A_i \chi_i, \tag{6}$$

where A_i is the hyperfine coupling field. Since the intrinsic susceptibility is temperature independent, the magnitude of A_s is not determined from the K–χ plot experimentally. A_{orb} is given by

$$A_{orb} = 2\mu_B \xi \langle r^{-3} \rangle, \tag{7}$$

where ξ is an orbital reduction factor. For $\xi = 1$, $A_{orb} = 84$ T/μ_B with $\langle r^{-3} \rangle = 6.699$ au [20]. In the tight-binding approximation, $(T_1T)^{-1}$ is written as [23]

$$(T_1T)^{-1} = (T_1T)_s^{-1} + (T_1T)_{orb}^{-1} + (T_1T)_{dip}^{-1}, \tag{8}$$

where the last term is the contribution from dipole interaction. For the a_{1g} orbital, each component can be obtained from two hyperfine fields of A_s and A_{orb}, and the density of states $N(E_F)$. On the reasonable assumption that $A_s > 0$ with a significant spin–orbit coupling [16] and $0.6 \leqslant \xi \leqslant 1$ [20, 23], the isotropic spin and orbital components of χ_i, K_i and A_i are estimated as follows: with $g = 2.24$ as the ESR value for the triangular lattice $Na_{0.09}CoO_2$ [10] and $\xi = 0.6$, $\chi_s = 1.4 \times 10^{-4}$ emu mol^{-1}, $K_s = 0.059\%$, $A_s = 2.4$ T/μ_B; and $\chi_{orb} = 2.8 \times 10^{-4}$ emu mol^{-1}, $K_{orb} = 2.54\%$. These parameters lead to the $(T_1T)^{-1}$ components of $(T_1T)_s^{-1} = 0.019$, $(T_1T)_{orb}^{-1} = 5.8$ and $(T_1T)_{dip}^{-1} = 1.0$ s^{-1} K^{-1}, which roughly account for the experimental value. The hyperfine field A_{so} induced by the spin–orbit interaction is then 12.4 T/μ_B, from the relation of $A_{so} = (g-2)A_{orb}$ [24], which provides the same A_s as that presented above for the usual core spin polarization value of -10 T/μ_B. Here, it should be noted that the $(T_1T)^{-1}$ value measured may not be isotropic, but is for the quantized axis direction. So, the above estimation may be altered a little obtaining the isotropic component of $(T_1T)^{-1}$. Through the rather simple analysis of NMR results, the spin susceptibility is found to agree with the value with $N(E_F) \approx 4.5$ eV^{-1} for CoO_2 (O1) [15], which is consistent with the picture that the present compound is a weakly correlated metal. A similar NMR analysis has been applied for the perovskite-type metal $SrVO_3$ [25].

3.4. NMR of ^{7}Li

For CoO_2 (P3)#1 and #2 that have the minor phases of O3-type Li_xCoO_2 and spinel-type Co_3O_4, respectively, the NMR spectra of ^{7}Li are observed at $\nu_L = 14.1$ MHz. The lineshapes are single Lorentzian and the NMR magnetizations exhibit a single-exponential recovery. The temperature dependences of Knight shifts and spin–lattice relaxation rates are shown in figures 5(a) and (b), respectively. The Knight shift for #1 is zero within an experimental error, which indicates that the outer s electrons of Li are absent, and T_1^{-1} is nearly temperature independent, as indicated by the dashed line. These results seem to correspond to those for the slow component of two kinds of relaxation processes for O3-type Li_xCoO_2 with $x \approx 0.92$ [26].

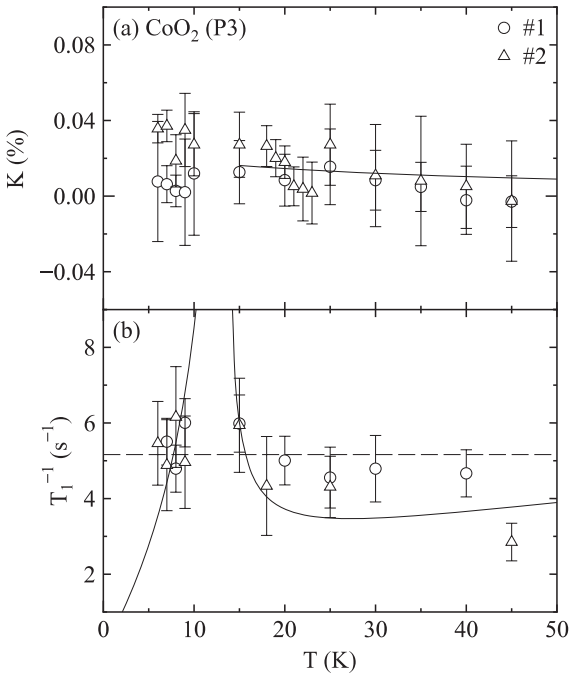

Figure 5. The temperature dependences of (a) the Knight shifts and (b) the spin–lattice relaxation rates of ^{7}Li nuclei in the minor phases of CoO_2 (P3)#1 and #2. The full curve for #2 in (a) is drawn based on the transferred hyperfine field for the Li-intercalated Co_3O_4 and that in (b) indicates fits to the SCR model.

As described in section 3.2, the minor phase of CoO_2 (P3)#2 may exhibit antiferromagnetism with $T_N \simeq 15$ K. The Knight shift seems to increase slightly with decreasing temperature, which may be caused by a transferred hyperfine field A_{tr} from Co^{2+} with $g = 2.17$ in Co_3O_4. The full curve in figure 5(a) provides $A_{tr} = 1.8(3) \times 10^{-3}$ T/μ_B. T_1^{-1} appears to increase with decreasing temperature above T_N. For a weak antiferromagnetism, it is known that the self-consistent-renormalization (SCR) theory gives the following characteristic temperature dependences of T_1^{-1} [27]: for $T > T_N$, $T_1^{-1} \propto T(T - T_N)^{-1/2}$; and for $T < T_N$, $T_1^{-1} \propto T(T_N - T)^{-1/2}$. The full curves drawn, based on this theory, in figure 5(b) may account for the experimental results. Therefore, the present results of Li may be for the slightly Li-intercalated Co_3O_4.

4. Conclusions

Stacking faults and metallic properties for the triangular lattice system CoO_2, which has basically three oxygen layers with

a prismatic oxygen environment between the layers, prepared through a chemical extraction of Li from $LiCoO_2$ with H_2SO_4, have been investigated mainly through measurements of NMR and NQR. A wide distribution of the quadrupole frequency for ^{59}Co nuclei due to the stacking fault and the short atomic coherence is found. The spin dynamics is successfully understood in terms of the relaxation mechanism for a weakly correlated metal system. The absence of antiferromagnetic spin fluctuations in two dimension suggests that the interaction between the CoO_2 layers is not so small. The Li ions contained in the present specimens are found to come from minor phases of O3-type Li_xCoO_2 with $x \approx 0.92$ or Li-intercalated spinel-type Co_3O_4.

For an application to rechargeable Li batteries with the use of transition-metal oxides, it is generally known that structural instabilities or phase separations, for undergoing intercalation and de-intercalation with Li ions, often give rise to a serious problem such as a lowering of discharge–charge cycle performance. The Li de-intercalated CoO_2 (P3), prepared soft-chemically, is rather stable to air exposure and metallic, and the stacking faults may relax the structural instabilities for the rigid lattice. Therefore, if the high voltage state of CoO_2 is first prepared by the soft-chemistry method, several chemical instabilities in the discharge and charge processes, related to the reduction and oxidation of the CoO_2 lattice, respectively, would be removed to a certain extent. This may produce high capacity batteries and application research on this viewpoint is highly desired.

References

[1] Anderson P W 1973 *Mater. Res. Bull.* **8** 153
[2] Fazekas P and Anderson P W 1974 *Phil. Mag.* **30** 423
[3] Takada K, Sakurai H, Takayama-Muromachi E, Izumi F, Dilanian R A and Sasaki T 2003 *Nature* **422** 53
[4] Terasaki I, Sasago Y and Uchinokura K 1997 *Phys. Rev.* B **56** R12685
[5] Onoda M and Ikeda T 2007 *J. Phys.: Condens. Matter* **19** 186213 and references therein
[6] Foo M L, Wang Y, Watauchi S, Zandbergen H W, He T, Cava R J and Ong N P 2004 *Phys. Rev. Lett.* **92** 247001
[7] Onoda M and Kikuchi Y 2007 *J. Phys.: Condens. Matter* **19** 346206
[8] See, for example, Antolini E 2004 *Solid State Ion.* **170** 159 and references therein
[9] Amatucci G G, Tarascon J M and Klein L C 1996 *J. Electrochem. Soc.* **143** 1114
[10] Onoda M and Sugawara A 2008 *J. Phys.: Condens. Matter* **20** 175207 and references therein
[11] de Vaulx C, Julien M-H, Berthier C, Hébert S, Pralong V and Maignan A 2007 *Phys. Rev. Lett.* **98** 246402
[12] Kawasaki S, Motohashi T, Shimada K, Ono T, Kanno R, Karppinen M, Yamauchi H and Zheng G 2009 *Phys. Rev.* B **79** 220514R in which the NMR results are suggested to be more reliable than those in [11]
[13] Roth W L 1964 *J. Physique* **25** 507
[14] Kundig W, Kobelt M, Appel H, Constabaris G and Lindequist R H 1969 *J. Phys. Chem. Solids* **30** 819
[15] Lee K-W and Pickett W E 2005 *Phys. Rev.* B **72** 115110
[16] Onoda M, Takao K and Ikeda T 2009 *Physica* C **469** 162 and references therein
[17] Das T P and Hahn E L 1958 *Solid State Phys.* **1** (Suppl.) 1
[18] Cohen M H and Reif F 1957 *Solid State Phys.* **5** 322
[19] See, for example, Creel R B, Segel C L, Schoenberger R J, Barnes R G and Torgeson D R 1974 *J. Chem. Phys.* **60** 2310 and references therein
[20] Abragam A and Bleaney B 1970 *Electron Paramagnetic Resonance of Transition Ions* (Oxford: Clarendon)
[21] Slichter C P 1963 *Principles of Magnetic Resonance* (New York: Harper and Row)
[22] Chepin J and Ross J H 1991 *J. Phys.: Condens. Matter* **3** 8103
[23] Yafet Y and Jaccarino V 1964 *Phys. Rev.* **133** A1630
[24] Onoda M, Takahashi T and Nagasawa H 1982 *J. Phys. Soc. Japan* **51** 3868
[25] Onoda M, Ohta H and Nagasawa H 1991 *Solid State Commun.* **79** 281
[26] Onoda M and Saito Y 2009 *Meet. Abstr. Phys. Soc. Japan* **64** 591
[27] Moriya T and Ueda K 1974 *Solid State Commun.* **15** 169